Pergamon

Int. J. Solids Structures Vol. 34, No. 17, pp. 2087–2103, 1997

Printed in Great Britain
0020–7683/97 $17.00 + .00

PII: S0020–7683(96)00133–3

ANALYSIS OF DYNAMIC CRACK PROPAGATION USING A TIME-DOMAIN BOUNDARY INTEGRAL EQUATION METHOD

TH. SEELIG and D. GROSS
Institute of Mechanics, TH Darmstadt, Hochschulstrasse 1, D-64289 Darmstadt, Germany

(*Received* 8 *February* 1996; *in revised form* 2 *July* 1996)

Abstract—Presented in this paper is a boundary element method which enables the simulation of dynamic crack propagation under arbitrary loading conditions and without any *a priori* assumptions regarding the crack path. The direction and speed of crack advance are controlled only by a fracture criterion. Fast crack growth is investigated in an unbounded linear elastic body under plane strain or longitudinal shear. For in-plane deformation under mixed mode loading the influence of crack closure on the computed crack path is considered by solving the related contact problem.

The starting point is a non-hypersingular time-domain traction boundary integral equation. A collocation method in conjunction with a time-stepping scheme is applied to solve the integral equation numerically. The accuracy of the numerical method is checked by comparison with analytical solutions available for simple situations. Some examples of curved cracks propagating with variable speed in inhomogenous stress fields serve to illustrate the versatility of the method.

1. INTRODUCTION

Several numerical studies of dynamic crack propagation have been published during the past two decades. But nearly all of them were restricted to a prescribed straight crack path. However, in reality cracks are often curved and they may kink or branch. Therefore, within the scope of a realistic model of these fracture processes the temporal and spatial evolution of a crack should be controlled only by a physically meaningful fracture criterion. Thus, the initial boundary value problem (IBVP) describing dynamic crack propagation is generally a free boundary value problem, since a part of the boundary varies with time and has to be determined from the analysis.

Linear elastodynamics which to some extent is adequate for brittle materials allows the formulation of IBVPs by time-domain boundary integral equations (see e.g. Eringen and Suhubi, 1975). Their numerical treatment by boundary element methods (BEMs) in contrast to methods of domain discretization (finite elements, finite differences) offers the advantages of a reduced dimension of the problem and an easy representation of arbitrarily curved and moving boundaries (crack paths). Nevertheless, in the few existing works using a BEM approach, these advantages have hardly been exploited. Standard BEMs can be applied within the subregion technique (Mettu and Kim, 1991; Gallego and Dominguez, 1992), but it is restricted to fixed crack paths and additional numerical expense results from introducing ficticious boundaries. For an efficient treatment of arbitrary crack paths it is necessary to represent the crack by a singular surface in the interior of a body as was done for example by Hirose and Achenbach (1991) and Koller *et al.* (1992). But the discretization chosen in Hirose and Achenbach (1991) requires some self-similarity and is not suited to model the growth of curved cracks. To our knowledge, the work of Koller *et al.* (1992) is the only approach by a BEM general enough to treat curvilinear dynamic crack growth. In their paper the propagation of a longitudinal shear crack in an unbounded domain has been investigated up to the formation of a first kink, indicating instability of the initially straight crack path.

The aim of our paper is to present a time-domain boundary element method for the simulation of rather general dynamic crack propagation problems. No restrictions are imposed on loading conditions or the shape of the developing cracks. Therefore, crack

closure and its influence on the fracture process has also been taken into account. In Section 2 we start with the derivation of the underlying boundary integral equation (BIE) for the unknown displacement discontinuity along a single crack which is growing with time in an unbounded domain. BIEs of the type used here are non-hypersingular and have been introduced by Zhang (1991) for the treatment of dynamically loaded stationary cracks. For simplicity we consider only two-dimensional problems of plane strain and longitudinal shear. Similar to the approach of Koller *et al.* (1992) the curvilinear crack is discretized by straight elements of constant length the number of which increases with time (Section 3). The unknown displacement jump is approximated by spatial and temporal splines. In each time step the BIE is solved on the current crack by a collocation method. To avoid a kinematically inadmissible penetration of the crack faces, in case of crack closure a contact problem has to be solved additionally. Via a penalty method the system of linear algebraic equations arising from the BIE is then extended to a nonlinear system and solved iteratively. The explicit time-stepping scheme resulting finally is typical for time-domain BEMs (see e.g. Zhang and Achenbach, 1989; Zhang and Gross, 1993). A fracture criterion connecting the dynamic stress intensity factors (SIFs) at the moving crack tip with the material's fracture toughness is applied in Section 4. In each time step it is evaluated to determine the direction and the speed of crack advance. Crack growth is modeled by adding new elements of constant length to the moving crack tip. As a consequence, no remeshing procedure is necessary, but the fracture criterion has to be discretized appropriately. 'Moving boundary elements' as applied by Gallego and Dominguez (1992) to describe the propagation of straight cracks seem not to be suited for curved cracks and would cause additional numerical expense through remeshing. Numerical results to test the accuracy of the method and to demonstrate its capability are presented in Section 5. Finally, conclusions are summarized in Section 6.

2. NON-HYPERSINGULAR TIME-DOMAIN BIE FOR PROPAGATING CRACK

From the basic equations of linear elastodynamics (Achenbach, 1973; Eringen and Suhubi, 1975) and zero initial conditions the following two-state 'conservation integral' can be derived (Zhang, 1991):

$$\int_{\partial B} \{\sigma_{ij}^{(2)} * (u_{i,j}^{(1)} n_k - u_{i,k}^{(1)} n_j) + \rho u_i^{(2)} * \ddot{u}_i^{(1)} n_k - u_{i,k}^{(2)} * \sigma_{ij}^{(1)} n_j\} \mathrm{d}A \equiv \int_B \rho (f_i^{(2)} * u_{i,k}^{(1)} + f_i^{(1)} * u_{i,k}^{(2)}) \mathrm{d}V. \tag{1}$$

Here ρ, u_i, σ_{ij}, and f_i denote the mass density and the components of displacement, stress, and body force, respectively, and B represents an arbitrary volume enclosed by its boundary ∂B with exterior unit normal n_i. Superscripts (1) and (2) denote two independent 'elastodynamic states' (of the same body), that means solutions of the field equations with zero initial conditions. Superscript dots and $(.)_{,j}$ indicate derivatives with respect to time and the spatial variables x_j. An asterisk $(*)$ denotes convolution with respect to time and the conventional summation rule over double indices is applied.

The integral identity (1) can be regarded as an alternative to the classical reciprocal theorem of elastodynamics (Betti–Rayleigh theorem; see e.g. Achenbach, 1973; Eringen and Suhubi, 1975), both being valid under the same conditions. As is well known, traction boundary integral equations (i.e. tractions given, displacements unknown) derived from the Betti–Rayleigh theorem become hypersingular when applied to cracks. To avoid this source of analytical and numerical difficulties Zhang (1991) proposed to take eqn (1) as the starting point instead. The succeeding steps which are the same as in the conventional approach and lead to a non-hypersingular BIE are outlined briefly. The first state in eqn (1) is chosen to be the unknown fields u_i, σ_{ij} with $f_i^{(1)} = 0$, and the second state is the fundamental solutions (elastodynamic Green's functions) $u_{il}^G(\mathbf{x}, \mathbf{y}, t-\tau)$ and $\sigma_{ijl}^G(\mathbf{x}, \mathbf{y}, t-\tau)$

due to an impulsive point force $\rho f_{il}^{(2)} = \delta(\mathbf{x}-\mathbf{y})\delta(t-\tau)\delta_{il}$ where $\delta(.)$ denotes Dirac's delta-distribution and δ_{il} is the Kronecker symbol. Insertion of the two states into eqn (1) gives the following representation formula for the displacement gradient in the interior of B:

$$\int_{\partial B}\{\sigma_{ijl}^{G} * (n_k\partial_j - n_j\partial_k)u_i^- - u_{il,k}^{G} * \sigma_{ij}^- n_j + \rho u_{il}^{G} * \ddot{u}_i^- n_k\}\,\mathrm{d}A(\mathbf{y}) = \begin{cases} u_{l,k}(\mathbf{x},t), & \mathbf{x}\in B\backslash\partial B \\ 0, & \mathbf{x}\in R^3\backslash(B\cup\partial B)\end{cases}\Bigg\}. \tag{2}$$

The boundary data u_i^- and σ_{ij}^- are the one-sided limits of the fields approaching ∂B from its interior. Note that the spatial derivative of u_i^- contains only a contribution tangential to ∂B. Adding to eqn (2) the representation formula for $u_{l,k}$ in the exterior domain (obtained in the same manner) and applying Hooke's law leads to the following representation formula for stress in the full space:

$$\sigma_{pq}(\mathbf{x},t) = -C_{pqkl}\int_{\partial B}\{\rho u_{il}^{G} * \Delta\ddot{u}_i n_k + \sigma_{ijl}^{G} * (n_k\partial_j - n_j\partial_k)\Delta u_i - u_{il,k}^{G} * \Delta\sigma_{ij} n_j\}\,\mathrm{d}A(\mathbf{y}), \quad \mathbf{x}\in R^3\backslash\partial B. \tag{3}$$

Here C_{pqkl} represents the elasticity tensor and $\Delta\varphi = \varphi^+ - \varphi^-$ denotes the jump of the field quantity φ over ∂B. The state of stress $\sigma_{pq}(\mathbf{x},t)$ resulting from discontinuous displacements and/or tractions along the arbitrary closed surface ∂B is sometimes called the scattered field.

A growing crack can generally be described by an open surface $\Gamma(t)$ along which the displacement field is discontinuous and the stress vector is continuous (it is zero for an open crack). Taking $\Gamma(t)$ as a part of ∂B, whereas all the fields must be continuous along the remainder of ∂B restricts the spatial integration in eqn (3) to the crack and makes the last term vanish.

The initial boundary value problem to be treated here is that of a crack growing with time in an unbounded domain. Initially the material is at rest and for $t > 0$ it is subject to some given loading, for example due to incident waves, represented by a stress field $\sigma_{pq}^{\mathrm{in}}(\mathbf{x},t)$. The crack itself is assumed to be free of traction. Superposition of the scattered field with the given loading, applying the traction free boundary condition along $\Gamma(t)$

$$\{\sigma_{pq}(\mathbf{x},t) + \sigma_{pq}^{\mathrm{in}}(\mathbf{x},t)\}n_q(\mathbf{x}) = 0, \quad \mathbf{x}\in\Gamma(t)$$

and taking the limit process $\mathbf{x}\to\Gamma(t)$ yields the following BIE for the unknown displacement jump along $\Gamma(t)$

$$\sigma_{pq}^{\mathrm{in}}(\mathbf{x},t)n_q(\mathbf{x}) = C_{pqkl}n_q(\mathbf{x})\,\Phi\!\!\!\!\!\!-\!\!\!\!\!\!\int_{\Gamma(t)}\int_0^t \{\rho u_{il}^{G}(\mathbf{x},\mathbf{y},t-\tau)\Delta\ddot{u}_i(\mathbf{y},\tau)n_k(\mathbf{y}) + \sigma_{ijl}^{G}(\mathbf{x},\mathbf{y},t-\tau)(n_k(\mathbf{y})\partial_j - n_j(\mathbf{y})\partial_k)\Delta u_i(\mathbf{y},\tau)\}\,\mathrm{d}\tau\,\mathrm{d}A(\mathbf{y}), \quad \mathbf{x}\in\Gamma(t). \tag{4}$$

The integral over $\Gamma(t)$ in eqn (4) does not contain any hypersingularities, it exists in the Cauchy principal value sense. But it contains derivatives of the unknown function and (4) therefore, strictly speaking, is an integro-differential equation. Of course, at any time τ the displacement is discontinuous only along the crack contour $\Gamma(\tau)$ existing at that instant. This fact later has to be reflected in an appropriate spline approximation of $\Delta u_i(\mathbf{y},\tau)$.

Derived under the assumption of traction free crack faces BIE (4) also holds in the case of crack closure when the additionally acting crack face pressure is formally included in the loading $\sigma_{pq}^{\mathrm{in}}(\mathbf{x},t)$. Of course this contact pressure is unknown and has to be determined from the condition of vanishing material penetration (see Section 3.2).

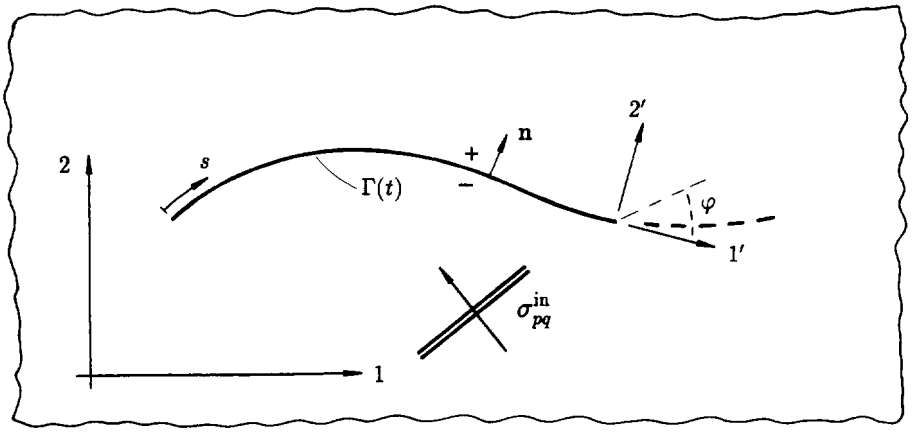

Fig. 1. Growing crack in 1,2-plane.

In the following we will restrict the analysis to two-dimensional problems and one-sided propagation of the crack. It then can be described by a curve $\Gamma(t)$ with arc length s, measured from the fixed crack tip (Fig. 1). The BIE (4) then reduces to

$$\sigma^{in}_{\alpha\beta}(\mathbf{x},t)n_\beta(\mathbf{x}) = C_{\alpha\beta\delta\varepsilon}n_\beta(\mathbf{x}) \oint_{\Gamma(t)} \int_0^t \left\{ \rho u^G_{\nu\varepsilon}(\mathbf{x},\mathbf{y},t-\tau)\Delta\ddot{u}_\nu(\mathbf{y},\tau)n_\delta(\mathbf{y}) + \mathbf{e}_{\gamma\delta}\sigma^G_{\nu\gamma\varepsilon}(\mathbf{x},\mathbf{y},t-\tau)\frac{\partial\Delta u_\nu(\mathbf{y},\tau)}{\partial s}\right\} \mathrm{d}\tau\,\mathrm{d}s(\mathbf{y}), \quad \mathbf{x}\in\Gamma(t) \tag{5}$$

in plane strain and to

$$\sigma^{in}_{3\beta}(\mathbf{x},t)n_\beta(\mathbf{x}) = \mu n_\beta(\mathbf{x}) \oint_{\Gamma(t)} \int_0^t \left\{ \rho u^G_{33}(\mathbf{x},\mathbf{y},t-\tau)\Delta\ddot{u}_3(\mathbf{y},\tau)n_\beta(\mathbf{y}) + \mathbf{e}_{\gamma\beta}\sigma^G_{3\gamma3}(\mathbf{x},\mathbf{y},t-\tau)\frac{\partial\Delta u_3(\mathbf{y},\tau)}{\partial s}\right\} \mathrm{d}\tau\,\mathrm{d}s(\mathbf{y}), \quad \mathbf{x},\in\Gamma(t) \tag{6}$$

in longitudinal shear. Here $\mathbf{e}_{\gamma\beta}$ denotes the two-dimensional permutation symbol and μ is the shear modulus. The 2-D Green's functions are given in Appendix A.

3. NUMERICAL SOLUTION PROCEDURE

3.1. *Boundary element method and time-stepping scheme*

To discretize the space–time domain of integration in BIEs (5) and (6), equidistant time steps Δt are chosen for the current time t and the past τ appearing in the time convolution:

$$t \to t_m = m\Delta t, \quad \tau \to \tau_n = n\Delta t, \quad n = 0,\ldots,m.$$

The crack at time t_m is approximated by an open polygon

$$\Gamma(t) \to \Gamma(t_m) = \bigcup_{e=1}^{E(m)} \Gamma_e$$

consisting of elements Γ_e of constant length Δy and nodal points $\mathbf{y}_e$ $(e = 0,\ldots,E(m))$

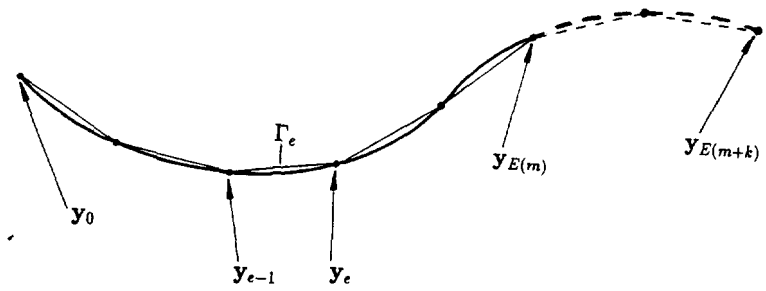

Fig. 2. Discretized crack.

(Fig. 2). The number of crack elements $E(m)$ increases with time (m) since crack growth is modeled by adding new elements to the moving crack tip.

The unknown crack opening displacements Δu_i are approximated using continuous piecewise linear temporal and piecewise continuous spatial interpolation functions

$$\Delta u_i(\mathbf{y},\tau) \cong \sum_{n=1}^{m}\sum_{e=1}^{E(n)} \phi_i^{ne}\eta_n(\tau)H_e(\mathbf{y})g_e(\mathbf{y}) \tag{7}$$

with

$$\eta_n(\tau) = \begin{cases} 1-\dfrac{|\tau-n\Delta t|}{\Delta t}, & \dfrac{\tau}{\Delta t}\in[n-1,n+1] \\ 0, & \text{otherwise} \end{cases} \tag{8}$$

$$= \frac{1}{\Delta t}\sum_{i=-1}^{1}(-2)^{(1-i^2)}(\tau-(n+i)\Delta t)H(\tau-(n+i)\Delta t)$$

and

$$H_e(\mathbf{y})g_e(\mathbf{y}) = \begin{cases} g_e(\mathbf{y}), & \mathbf{y}\in\Gamma_e \\ 0, & \text{otherwise} \end{cases} \quad (H(.) \triangleq \text{Heaviside function}). \tag{9}$$

The unknown coefficients ϕ_i^{ne} are the displacement jumps at the element midpoints at discrete times τ_n. To describe the proper asymptotic behaviour at the crack tips $(r\to 0)$ 'square root' shape functions

$$g_e(\mathbf{y}) \sim \sqrt{r}, \quad r\text{: distance from crack tip} \tag{10}$$

are used on the first two elements behind each crack tip, whereas on the remaining 'inner' elements $g_e(\mathbf{y}) \equiv 1$.

The spatial shape functions at the moving crack tip also depend on time, when expressed in global coordinates $\mathbf{y}$ and the location $\mathbf{a}(\tau)$ of the crack tip at time τ:

$$g_e(\mathbf{y}) \sim \sqrt{r} = \sqrt{|\mathbf{a}(\tau)-\mathbf{y}|}.$$

Strictly speaking this has to be taken into account when performing the time differentiation of eqn (7) and the time convolution as was already mentioned by Gallego and Dominguez (1992). But being confirmed by our numerical results we neglect this time dependence by regarding the crack tip motion as a series of discrete locations:

$$g_e(\mathbf{y}) \sim \sqrt{r} = \sqrt{|\,\mathbf{a}(\tau_n)-\mathbf{y}\,|} \quad \text{for} \quad \mathbf{y}\in\Gamma(\tau_n) \quad \text{and} \quad \tau\in[\tau_{n-1},\tau_{n+1}]. \tag{11}$$

This is in consistency with modeling crack growth by adding new elements at discrete instants of time.

To solve the BIE approximately, the element midpoints $\mathbf{x}^d$ ($d = 1,\ldots,E(m)$) on the current crack $\Gamma(t_m)$ and the temporal nodal point t_m are taken as spatial and temporal collocation points which correspond to the polynomial degrees of the chosen interpolation functions (8) and (9). With auxiliary functions $V_{v\varepsilon}(\mathbf{y};\mathbf{x}^d,m,n,i)$ and $\Sigma_{v\gamma\varepsilon}(\mathbf{y};\mathbf{x}^d,m,n,i)$ resulting from the analytical evaluation of the time convolution (see Appendix B) the collocation method applied to BIE (5) leads to the following system of linear algebraic equations

$$\sigma_\alpha^{md} = \frac{\sigma_{\alpha\beta}^{\mathrm{in}}(\mathbf{x}^d,t_m)}{\mu}n_\beta(\mathbf{x}^d) = \sum_{n=1}^{m}\sum_{e=1}^{E(n)}\sum_{v=1}^{2}\phi_v^{ne}\frac{C_{\alpha\beta\delta\varepsilon}}{\mu}n_\beta(\mathbf{x}^d)\frac{\mathbf{e}_{\gamma\delta}}{2\pi c_T\Delta t}\sum_{i=-1}^{1}(-2)^{(1-i^2)}$$

$$\times \oint_{\Gamma(t_m)}\Bigg[V_{v\varepsilon}(\mathbf{y};\mathbf{x}^d,m,n,i)\tau_\gamma(\mathbf{y})H_e(\mathbf{y})g_e(\mathbf{y})$$

$$+\frac{1}{|\,\mathbf{y}-\mathbf{x}^d\,|}\Sigma_{v\gamma\varepsilon}(\mathbf{y};\mathbf{x}^d,m,n,i)\frac{\mathrm{d}}{\mathrm{d}s}(H_e(\mathbf{y})g_e(\mathbf{y}))\Bigg]\mathrm{d}s(\mathbf{y}) = \sum_{n=1}^{m}\sum_{e=1}^{E(n)}\sum_{v=1}^{2}\phi_v^{ne}A_{ne\alpha}^{mdv}. \tag{12}$$

Here $\tau_\gamma = \mathbf{e}_{\gamma\delta}n_\delta$ denotes the unit vector tangent to the crack and c_T is the shear wave velocity. The integral over $V_{v\varepsilon}(.)$ is only weakly singular at the wave fronts $|\,\mathbf{y}-\mathbf{x}^d\,| = c_{L/T}\Delta t(m-n-i)$, whereas the second part has to be evaluated in the Cauchy principal value sense (see e.g. Zhang and Gross, 1993). In the case of longitudinal shear BIE (6) leads to an analogous system of equations. Differentiation of the discontinuous spatial interpolation functions in eqn (12) has to be understood in the distributional sense with $(\mathrm{d}/\mathrm{d}s)H(s) = \delta(s)$:

$$\oint_{\Gamma(t_m)}\ldots\frac{\mathrm{d}}{\mathrm{d}s}(H_e(\mathbf{y})g_e(\mathbf{y}))\,\mathrm{d}s(\mathbf{y}) = \oint_{\Gamma_e}\ldots\frac{\mathrm{d}g_e}{\mathrm{d}s}(\mathbf{y})\,\mathrm{d}s(\mathbf{y}) - [\ldots g_e(\mathbf{y})]_{\mathbf{y}=\mathbf{y}_{e-1}}^{\mathbf{y}_e}. \tag{13}$$

The matrix elements $A_{ne\alpha}^{mdv}$ in eqn (12) represent the influence of the displacement jump component v on element Γ_e at a former time τ_n on the stress vector component α at collocation point $\mathbf{x}^d$ at the present time t_m. The respective matrices have a special structure determined by the hyperbolicity of the field equations, the chosen interpolation functions, and the collocation method, such that

$$A_{ne\alpha}^{mdv} \neq 0 \quad \text{only for} \quad \frac{1}{2}|\,e-d\,| < \frac{c_L\Delta t}{\Delta y}(m-n+1). \tag{14}$$

Decomposing system (12) into

$$\sigma_\alpha^{md} = \sum_{n=1}^{m-1}\sum_{e=1}^{E(n)}\sum_{v=1}^{2}A_{ne\alpha}^{mdv}\phi_v^{ne} + \sum_{e=1}^{E(m)}\sum_{v=1}^{2}A_{me\alpha}^{mdv}\phi_v^{me} \tag{15}$$

leads to the following time-stepping scheme

$$\phi_v^{me} = \sum_{d=1}^{E(m)}\sum_{\alpha=1}^{2}(A_{me\alpha}^{mdv})^{-1}\left(\sigma_\alpha^{md} - \sum_{n=1}^{m-1}\sum_{j=1}^{E(n)}\sum_{\gamma=1}^{2}A_{nj\gamma}^{md\gamma}\phi_\gamma^{nj}\right) \tag{16}$$

from which the coefficients ϕ_v^{me} unknown at current time t_m can be computed. The right hand side of eqn (16) consists of the given loading and a contribution from the past ($n < m$). In contrast to the situation of a stationary crack (Zhang and Achenbach, 1989; Zhang and

Gross, 1993) here the matrices $(A^{mdv}_{ne\alpha})$ depend on m and n not only through the difference $m-n$ (time-translation invariance, see Appendix B) but also through the temporally growing number of elements $E(n)$ and collocation points $E(m)$. Thus, in each time step (m) a matrix element $A^{mdv}_{ne\alpha}$ has to be computed if

$$n = 1 \quad \text{or} \quad e \geqslant E(n)-2 \quad \text{or} \quad d = E(m).$$

Otherwise its value is known from a previous time step. Because of condition (14) the matrices to be inverted in eqn (16) $(m = n)$ are banded. Furthermore, for $\Delta t \leqslant \Delta y/2c_L$ they consist only of 2×2-blocks along the 'diagonal' $e = d$, since waves emitted from one element (and traveling with velocities $c_L > c_T > c_R$) do not reach the midpoint (collocation point) of a neighbouring element during Δt. So, in the latter case the two components of the unknown displacement jump on each element depend only on the components of the right hand side of eqn (16) on the same element. Within the scope of the numerical procedure presented here the spatial and temporal element lengths Δy and Δt are subject to certain restrictions mostly based on numerical experiments. To ensure a good resolution of short-time effects it is necessary to choose $\Delta t \leqslant \Delta y/c_L$. But too small values of Δt may cause instabilities in the solution at large time as was already mentioned by Zhang and Achenbach (1989).

3.2. *Contact problem*

For in-plane deformation and arbitrary loading it may happen that a crack closes. Then the crack faces are no longer free of traction, but an additional contact pressure acts as a 'constraint force' to prevent the displacement jump normal to the crack from being negative (material penetration). This contact problem can be solved via a penalty method. For this purpose the *a priori* unknown contact pressure is formally considered to be part of the given loading, leading to the following extension of eqn (15) (no summation over d)

$$\sum_{e=1}^{E(m)} \sum_{\nu=1}^{2} A^{mdv}_{me\alpha} \phi^{me}_{\nu} = \sigma^{md}_{\alpha} + p^{md} n^{d}_{\alpha} - \sum_{n=1}^{m-1} \sum_{e=1}^{E(n)} \sum_{\nu=1}^{2} A^{mdv}_{ne\alpha} \phi^{ne}_{\nu}. \tag{17}$$

The contact pressure p^{md} at time t_m and collocation point $\mathbf{x}^d$ is assumed to be proportional to the kinematically inadmissible material penetration on element Γ_d with a penalty parameter c_p much bigger ($\times 10^3$) than the elastic stiffnesses contained in $A^{mdv}_{me\alpha}$:

$$p^{md} = c_p(|\phi^{md}_{n}| - \phi^{md}_{n}), \quad \phi^{md}_{n} = \sum_{\nu=1}^{2} \phi^{md}_{\nu} n^{d}_{\nu}. \tag{18}$$

Thus, the contact pressure is only nonzero when ϕ^{md}_{n} the displacement jump normal to the crack is negative. With p^{md} inserted, eqn (17) becomes a system of nonlinear algebraic equations which is solved iteratively by a Newton method. The iteration is started (only if necessary) using the solution obtained under the assumption of an open and traction free crack. Due to the bilinearity of the stiffness the method converges in two steps.

As already mentioned, for small time steps $\Delta t \leqslant \Delta y/2c_L$ the system (15) or (17) decouples. That means, a contact pressure acting on one element only influences the solution ϕ^{me}_{ν} on the same element. From the condition that the material penetration vanishes the pressure on each element can be computed exactly by solving only a 2×2-system.

Throughout this work crack face contact was assumed to be frictionless, but taking into account a frictional stress depending on the contact pressure would produce no difficulty.

4. FRACTURE CRITERION AND MODELLING OF CRACK ADVANCE

From the computed displacement jumps near the running crack tip the dynamic stress intensity factors (SIFs) are determined as functions of time and the crack tip speed $\dot{a}$ (Freund, 1990):

$$K_{\mathrm{I}}(t;\dot{a}) = \frac{4\alpha_{\mathrm{L}}\alpha_{\mathrm{T}} - (1+\alpha_{\mathrm{T}}^2)^2}{4\alpha_{\mathrm{L}}(1-\alpha_{\mathrm{T}}^2)}\mu\sqrt{2\pi}\lim_{r\to 0}\frac{\Delta u_n(r,t)}{\sqrt{r}}$$

$$K_{\mathrm{II}}(t;\dot{a}) = \frac{4\alpha_{\mathrm{L}}\alpha_{\mathrm{T}} - (1+\alpha_{\mathrm{T}}^2)^2}{4\alpha_{\mathrm{T}}(1-\alpha_{\mathrm{T}}^2)}\mu\sqrt{2\pi}\lim_{r\to 0}\frac{\Delta u_t(r,t)}{\sqrt{r}}$$

$$K_{\mathrm{III}}(t;\dot{a}) = \frac{\alpha_{\mathrm{T}}}{4}\mu\sqrt{2\pi}\lim_{r\to 0}\frac{\Delta u_3(r,t)}{\sqrt{r}} \quad \text{with} \quad \alpha_{\mathrm{L,T}} = \sqrt{1-\left(\frac{\dot{a}}{c_{\mathrm{L/T}}}\right)^2}. \tag{19}$$

Here Δu_n and Δu_t denote the displacement jumps normal and tangential to the crack in case of inplane deformation and r is the distance from the crack tip. Because of the $\sqrt{r}$-crack tip shape functions (10) the SIFs depend only on the coefficients $\phi^{m,E(m)}$ on the crack tip element. From energy considerations it can be shown (Freund, 1990) that the crack tip speed is limited by the Rayleigh wave speed c_{R} for inplane deformation and by the shear wave speed c_{T} for longitudinal shear. The SIFs vanish when these limits are reached.

The SIFs enter the representation of the singular stress field at the moving crack tip (Fig. 1) from which the following components will be needed for the fracture criterion

$$\begin{aligned}\sigma_{\varphi\varphi}(r,\varphi,t;\dot{a}) = \frac{1}{\sqrt{2\pi r}}\{&(K_{\mathrm{I}}(t;\dot{a})\Sigma^{\mathrm{I}}_{1'1'}(\varphi;\dot{a}) + K_{\mathrm{II}}(t;\dot{a})\Sigma^{\mathrm{II}}_{1'1'}(\varphi;\dot{a}))\sin^2\varphi \\ &+ (K_{\mathrm{I}}(t;\dot{a})\Sigma^{\mathrm{I}}_{2'2'}(\varphi;\dot{a}) + K_{\mathrm{II}}(t;\dot{a})\Sigma^{\mathrm{II}}_{2'2'}(\varphi;\dot{a}))\cos^2\varphi \\ &- (K_{\mathrm{I}}(t;\dot{a})\Sigma^{\mathrm{I}}_{1'2'}(\varphi;\dot{a}) + K_{\mathrm{II}}(t;\dot{a})\Sigma^{\mathrm{II}}_{1'2'}(\varphi;\dot{a}))\sin 2\varphi\}\end{aligned} \tag{20}$$

$$\sigma_{3\varphi}(r,\varphi,t;\dot{a}) = \frac{K_{\mathrm{III}}(t;\dot{a})}{\sqrt{2\pi r}}(\Sigma_{32'}(\varphi;\dot{a})\cos\varphi - \Sigma_{31}(\varphi;\dot{a})\sin\varphi). \tag{21}$$

The universal functions $\Sigma(\varphi;\dot{a})$ can be found in Freund (1990) eqns (4.3.11), (4.3.24), and (4.2.17).

Here we employ the fracture criterion of Erdogan and Sih (1963). It states that crack advance will take place in the direction φ_0 of maximum circumferential stress $\sigma_{\varphi\varphi}$ when this stress reaches the same critical value as in pure mode I

$$\max\sigma_{\varphi\varphi}(\varphi;K_{\mathrm{I}},K_{\mathrm{II}}) - \sigma_{\varphi\varphi}(\varphi=0;K_{\mathrm{Ic}})\begin{cases}=0 & \text{for } \dot{a}>0\\ <0 & \text{for } \dot{a}=0\end{cases}. \tag{22}$$

For a propagating crack the value of $\dot{a}$ is such that the equality holds. The critical stress is represented by the dynamic fracture toughness $K_{\mathrm{Ic}} = K_{\mathrm{ID}}(\dot{a})$ which as a function of crack tip speed has to be determined experimentally. For mode III crack propagation the fracture criterion reads

$$\max\sigma_{3\varphi}(\varphi;K_{\mathrm{III}}) - \sigma_{3\varphi}(K_{\mathrm{IIIc}})\begin{cases}=0 & \text{for } \dot{a}>0\\ <0 & \text{for } \dot{a}=0\end{cases}. \tag{23}$$

Similar to the approach of Koller *et al.* (1992), crack growth is modeled by adding a new element of constant length Δy to the moving crack tip whenever condition (22) or (23) is violated. This can take place only after some time steps Δt have passed, because $\dot{a} < c_{\mathrm{R}} < c_{\mathrm{T}} < c_{\mathrm{L}} \leqslant \Delta y/\Delta t$. Thus, the crack tip moves by discrete jumps at times $t_{m_{k-1}}, t_{m_k}, \ldots$.

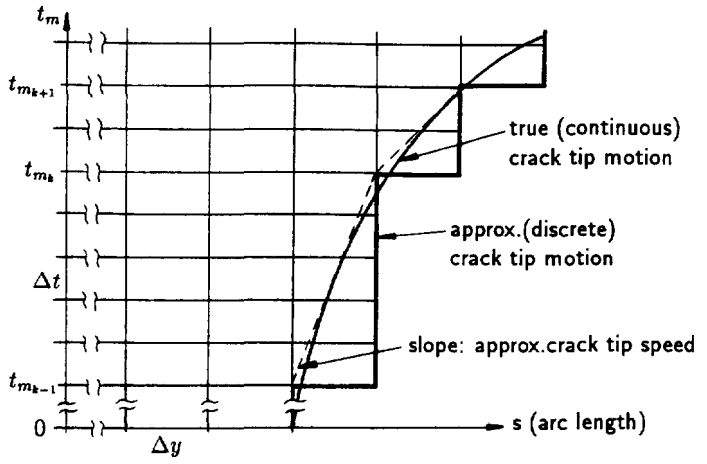

Fig. 3. Discrete modelling of crack tip motion.

Figure 3 shows the continuous motion of the crack tip and its discrete approximation. It can be seen that the numerical crack tip speed cannot be computed for each time step but only as the average value (dashed-line in Fig. 3) over the whole interval between two instants of discrete crack advance:

$$\dot{a}(t) \approx \frac{\Delta y}{t_{m_k} - t_{m_{k-1}}} = \frac{\Delta y}{\Delta t(m_k - m_{k-1})} \quad \text{for} \quad t \in [t_{m_{k-1}}, t_{m_k}]. \tag{24}$$

With $\Delta y/\Delta t c_L$ fixed, it is obvious from eqn (24) that $\dot{a}$ can take on only discrete values, because $m_k - m_{k-1}$ is an integer. As an example, for $\Delta y/\Delta t c_L = 1.5$ and $\dot{a} = 0.25\, c_L$ a crack tip jump of Δy takes place every six time steps ($m_k - m_{k-1} = 6$). For the same reason the dynamic SIFs (19) are averaged with respect to time before entering the fracture criterion. After the onset of crack growth ($\dot{a} > 0$)

$$K(t_m) = \frac{1}{(t_m - t_{m_k})} \int_{t_{m_k}}^{t_m} K(t)\, \mathrm{d}t \tag{25}$$

can be regarded to be the SIF consistent with the discretization as proposed by Koller *et al.* (1992). Here t_{m_k} is the last instant of discrete crack advance. To evaluate the fracture criterion at current time $t_m > t_{m_k}$ the crack tip speed is required in eqns (19)–(23). But, only available from eqn (24) for a time interval between two known instants of discrete crack advance, $\dot{a}$ has to be determined iteratively. Therefore at time t_m we first use for $\dot{a}$ the value obtained for the interval $[t_{m_{k-1}}, t_{m_k}]$. Violation of condition (22) or (23) seemingly indicates the necessity to add a new element. Thus, a new crack tip speed can now be computed for the interval $[t_{m_k}, t_m]$. Only if condition (22) or (23) evaluated with this new crack tip speed is violated, t_m is accepted to be a new instant $t_{m_{k-1}}$ of discrete crack growth. Then a new element having the direction φ_0 determined from the fracture criterion is added to the crack tip. Otherwise no crack advance takes place at that time and computations in the next time step (t_{m+1}) are performed using the old value for $\dot{a}$ again.

If, on the other hand, at t_m the time passed since the last crack tip jump becomes longer than corresponds to the value currently in use for $\dot{a}$, the crack tip speed is made topical according to

$$\dot{a} = \min\left(\dot{a}, \frac{\Delta y}{\Delta t(m - m_k)}\right). \tag{26}$$

This takes place when the crack slows down.

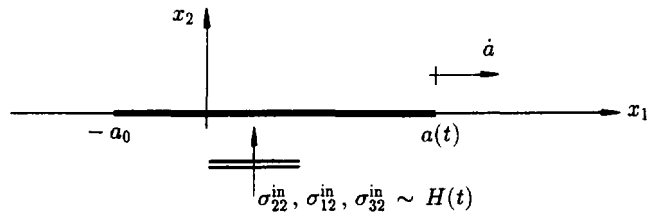

Fig. 4. One-sided propagation of straight crack loaded by plane waves.

5. NUMERICAL RESULTS

Before more general problems are treated the accuracy of the method is tested by comparison with analytical solutions available for some simple situations. All numerical computations reported in this paper are carried out with Poisson's ratio of $\nu = 0.25$ ($c_L = \sqrt{3}c_T, c_R = 0.92\ c_T$). The quantity $\Delta y/c_L\Delta t$ characterizing the discretization should be chosen from the interval [1, 2]. In all examples we start with a straight initial crack of length $2a_0$ along the x_1-axis. If not stated otherwise, it is discretized by 20 elements. No other quantities have to be specified since the shear modulus can be related to a stress amplitude of the loading, say σ^*, and the corresponding static stress intensity factor $K_{stat.} = \sigma^*\sqrt{\pi a_0}$ serves to normalize the dynamic SIFs and the dynamic fracture toughness.

5.1. *Comparison with analytical solutions*

Analytical solutions are available for the dynamic propagation of straight semi-infinite cracks loaded by constant stress (Freund, 1990). In case of a prescribed constant crack tip speed these solutions are the dynamic SIFs at the running crack tip for mode I, II and III. The 'inverse' problem for a mode III crack propagating according to the fracture condition of a constant energy release rate (ideal brittle fracture) has been solved analytically by Kostrov (1966) to give the unsteady motion of the crack tip in closed form. Numerically we examine the one-sided propagation of a finite crack (Fig. 4) loaded at $t = 0$ by normal incident plane waves carrying a jump of constant stress. After some time the stress field at one tip of the finite crack is influenced by waves emanating at $t = 0$ from the second crack tip. Beyond this time the numerical results cannot be compared any longer to the analytical solutions valid for semi-infinite cracks.

5.1.1. *Constant crack tip speed.* When the crack tip speed is prescribed, no fracture criterion has to be employed. The dynamic SIFs are computed from eqns (19) and (25)

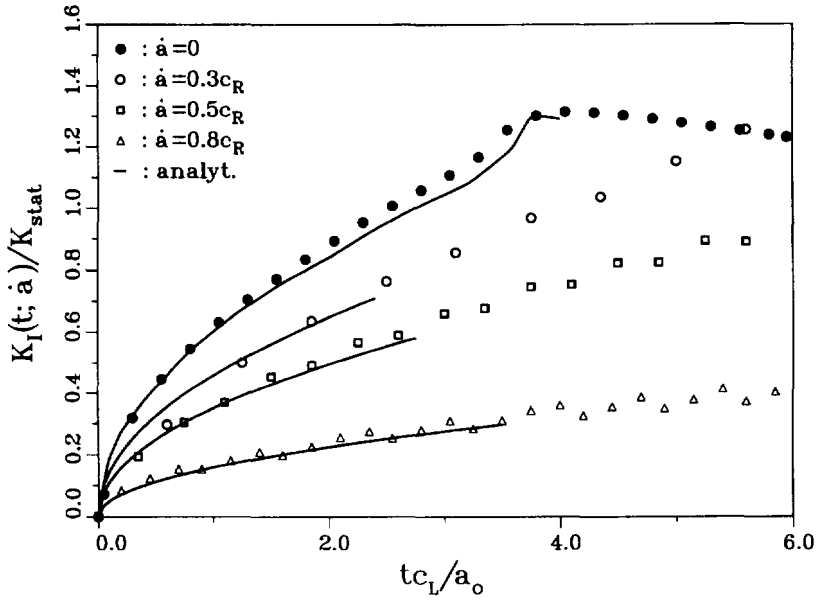

Fig. 5a. Mode I SIF at running crack tip.

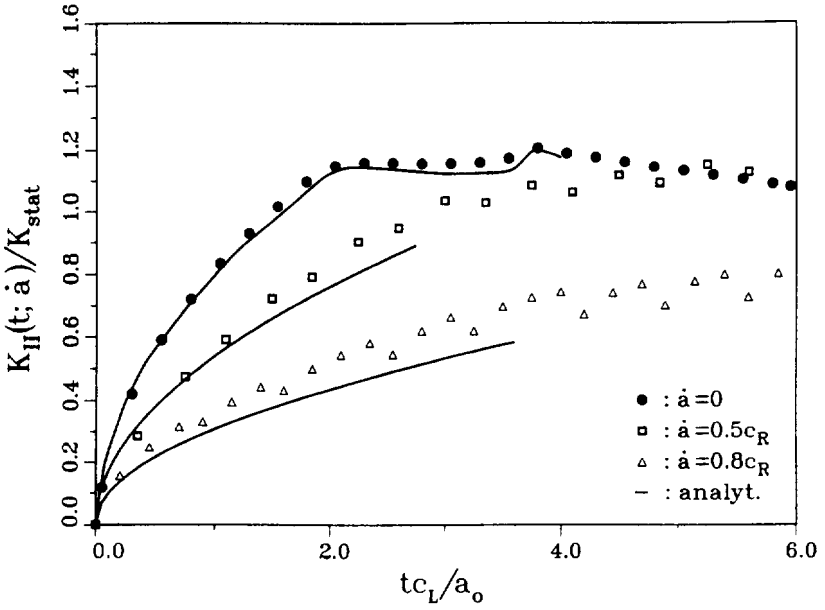

Fig. 5b. Mode II SIF at running crack tip.

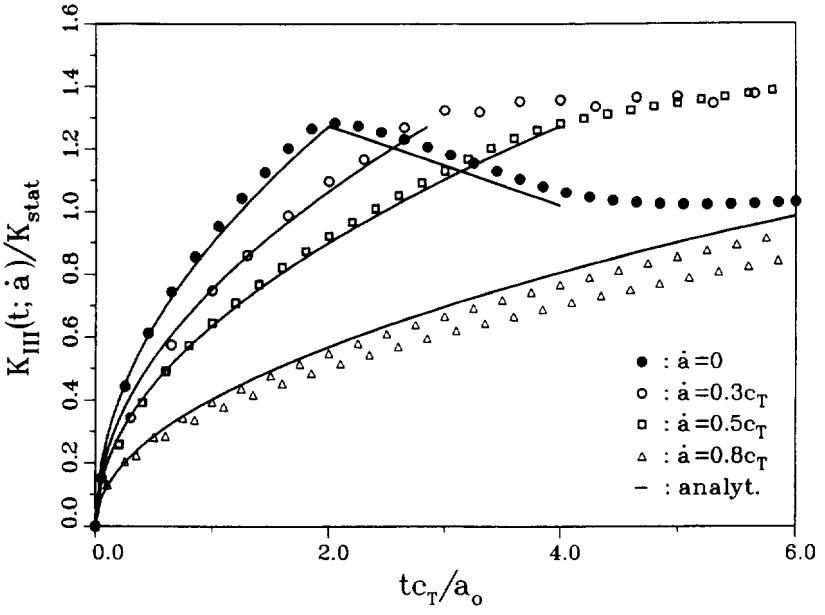

Fig. 5c. Mode III SIF at running crack tip.

whereas analytical solutions can be found in Freund (1990). For finite stationary cracks ($\dot{a} = 0$) analytical solutions taking into account a first interaction of the two crack tips are available from Thau and Lu (1971). Figures 5(a)–(c) show the normalized SIFs for mode I, II, and III vs dimensionless time for various values of the crack tip speed. In view of the simplicity of the numerical method the results are quite satisfactory.

The number of time steps taken for averaging the SIFs in eqn (25) decreases with increasing crack tip speed. Moreover, depending on the value of $\Delta y/\dot{a}\Delta t$ this number of time steps alternates from averaging period to averaging period. This results in some scattering in the averaged SIFs which can be seen for high crack tip speed, especially in Fig. 5(c). The mode II SIF is of minor importance since a real mixed mode loaded crack immediately forms a kink and tends to propagate under pure mode I conditions, as is known from experiments and reflected in the fracture criterion (22).

5.1.2. *Constant energy release rate, mode III crack.* For a constant energy release rate the critical SIF is $K_{IIIc} = K_{IIIc_0}(1-(\dot{a}/c_T)^2)^{1/4}$ (Kostrov, 1966). It enters the fracture criterion

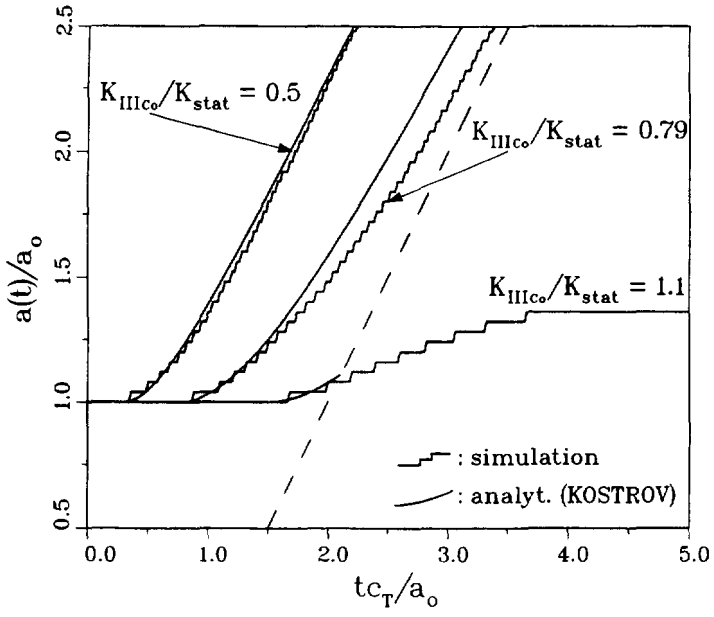

Fig. 6. Crack tip motion at constant energy release rate.

(23) and crack initiation takes place when $K_{III}(t; 0) = K_{IIIc_0}$. Figure 6 shows the crack tip motion along the x_1-axis computed via the algorithm described in Section 4 and the analytical solution of Kostrov (1966) for various values of K_{IIIc_0}. Also shown is the characteristic (dashed-line) of the first disturbance emanating from the fixed crack tip. It forms the boundary of the domain in the t,x_1-plane where the analytical solution (semi-infinite crack) is valid. Only for $K_{IIIc_0}/K_{stat} > 0.794$ this wave reaches the running crack tip, reducing the SIF and possibly leading to crack arrest. For smaller values of K_{IIIc_0} the crack tip speed asymptotically tends to the shear wave speed c_T. Here 50 elements were used to discretize the initial crack. Again the results are quite satisfactory and justify the application of the numerical method to more general problems.

5.2. *Curved crack growth*

From now on any restrictions on the crack path are released and only the physically more interesting situation of plane strain allowing for crack face contact is regarded. For the dynamic fracture toughness $K_D(\dot{a})$ the relation shown in Fig. 7 which is typical for steel and other moderately brittle materials is assumed (see measurements of Kalthoff and Rosakis *et al.* reported by Dally *et al.*, 1985). The steep increase in $K_D(\dot{a})$ acts like a barrier to $\dot{a}$ at about 0.4 c_T. It results from energy dissipation by micromechanisms not considered in detail on this macroscopic level. Because of that behaviour, the crack tip speed in the following examples is limited to the range for which the direction of crack advance computed

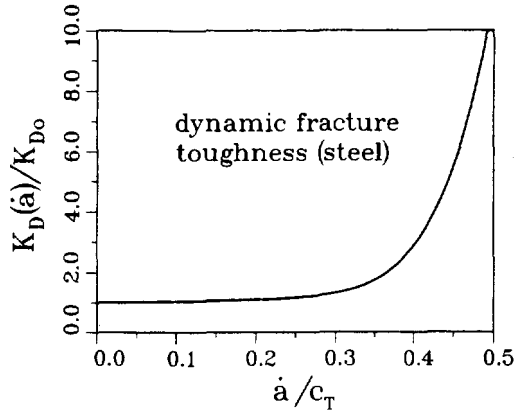

Fig. 7. Dynamic fracture toughness.

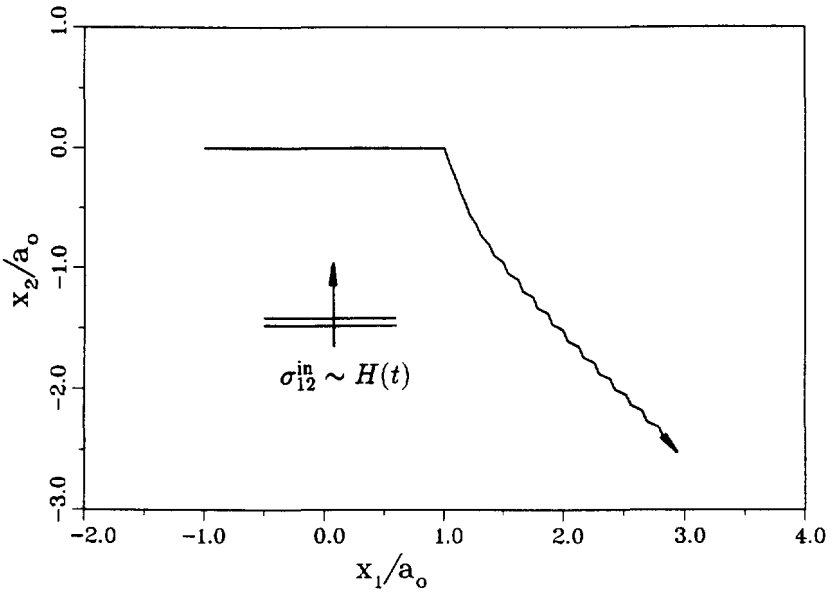

Fig. 8. Crack path due to shear wave loading.

from fracture criterion (22) remains unique. For $\dot{a} > 0.6\, c_R$ this uniqueness is lost (Freund, 1990).

5.2.1. *Loading by plane shear wave.* The initial crack is loaded by a normal incident plane wave of a constant shear stress jump (mode II). When condition (22) is violated the crack kinks by an angle of approximately 70° and then propagates in a slight bow (Fig. 8). This behaviour is well known from experiments performed under static loading conditions (Erdogan and Sih, 1963). Controlled by the fracture criterion the crack tends to propagate under pure mode I conditions the direction of which approaches 45° with increasing distance from the initial crack. Here no crack closure takes place. The crack tip speed after a short period of acceleration reaches a constant value determined by the magnitude of loading. For different magnitudes the resulting crack paths are nearly identical. So, dynamic effects seem to have little influence on crack propagation in unbounded domains as long as the direction of crack advance is unique. The zig-zag course of the crack path results from determining the direction of crack advance before a new element of finite length is added ('forward scheme').

5.2.2. *Center of dilatation.* To study dynamic crack propagation due to an inhomogeneous stress field the loading now is generated by a static center of dilatation given by $\boldsymbol{\sigma}^{in}(\mathbf{x}, t) = \boldsymbol{\sigma}^{D}(\mathbf{x})H(t)$ with

$$\sigma_{rr}^{D}(r, \varphi) = -\sigma^{*}\left(\frac{a_0}{r}\right)^2, \quad \sigma_{\varphi\varphi}^{D}(r, \varphi) = +\sigma^{*}\left(\frac{a_0}{r}\right)^2, \quad \sigma_{r\varphi}^{D}(r, \varphi) = 0. \tag{27}$$

Here the polar coordinates r and φ are related to the location of the r^{-2}-singularity. When a center of dilatation (•) is located beside the initial crack (Fig. 9) the crack is closed by the negative radial stress and crack initiation takes place under pure mode II conditions with the typical kinking angle of about 70°. In this case the related contact problem has to be solved as described in Section 3.2. When contact is neglected and material penetration is admitted the computed crack path may differ totally from the 'correct' one (Fig. 9). In both cases the kinking angle is the same, because $K_I = 0$ for the initial crack independently from considering crack face contact or not.

5.2.3. *Center of compression.* The stress field generated by a center of compression (•) (Fig. 10) is opposite to that of a center of dilatation and leads to spiral crack growth around

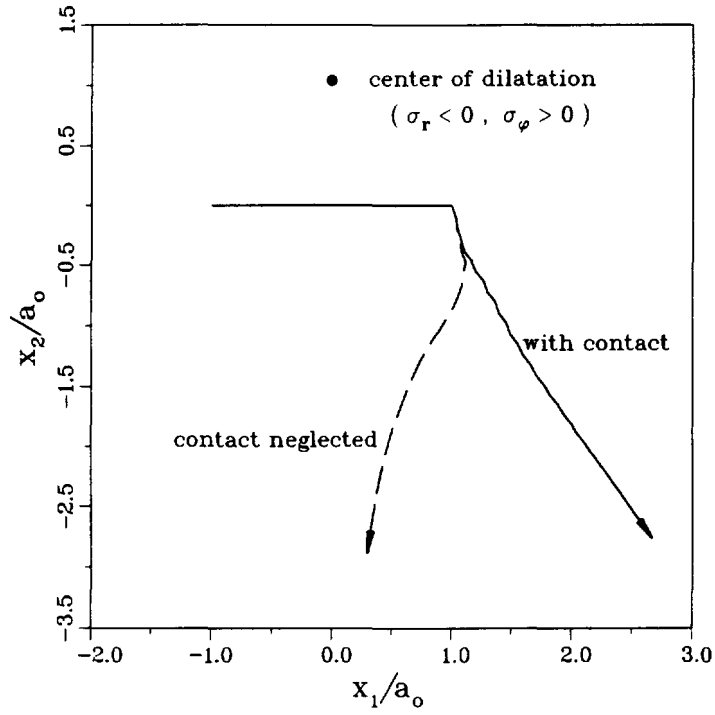

Fig. 9. Center of dilatation (•) beside initial crack.

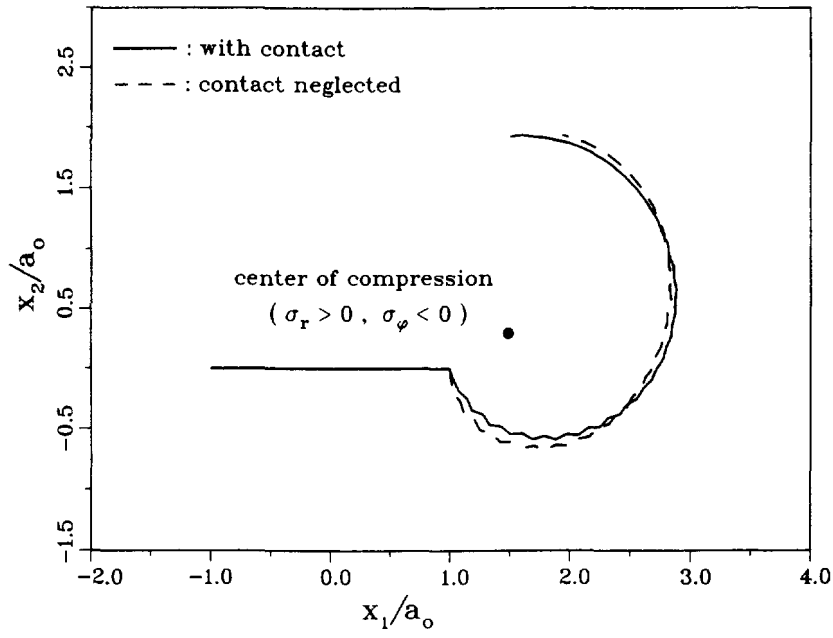

Fig. 10. Center of compression (•) in front of initial crack.

the nucleus of stress. Here the initial crack is closed by the negative circumferential stress. Consideration or neglection of crack face contact, again results in different crack paths obtained from the simulation. The 'correct' crack path again starts with an kinking angle of 70° because of pure mode II crack initiation. The larger angle in the other case results from a negative mode I SIF which is physically meaningless.

Additional information about the fracture process can be obtained from the crack tip speed and the dynamic mode I SIF. In the case of crack face contact correctly considered in the simulation these quantities are shown vs the amount of crack advance in Figs 11 and 12. Although the crack tip speed takes on only 'a few' discrete values (see Section 4), the short period of acceleration after crack initiation and the decrease in crack tip speed, leading

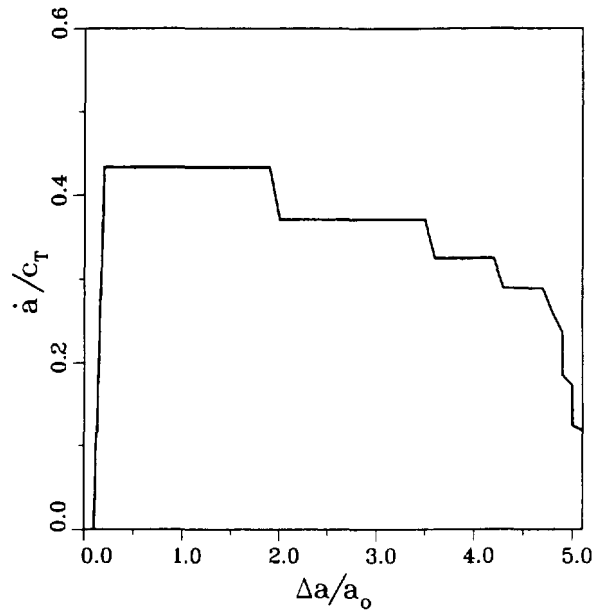

Fig. 11. Crack tip speed.

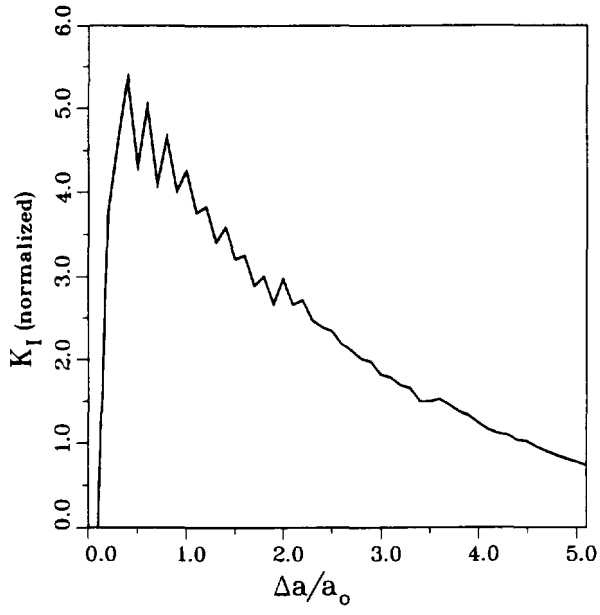

Fig. 12. Mode I SIF.

to crack arrest, can clearly be seen. The strong decrease in crack tip speed results not only from an increasing distance to the center of compression, but also from a change in geometry due to crack growth. The simulation here was stopped at $t = 27a_0/c_L$.

6. CONCLUSIONS

A numerical method has been presented, which enables the simulation of dynamic crack propagation under arbitrary loading conditions and along arbitrary crack paths. Since penetration of the crack faces is kinematically inadmissible, the treatment of the contact problem arising from crack closure is included in the procedure. Crack advance starting from a given initial crack is determined from a fracture criterion motivated by experimental observations. The method although being based on a rough approximation of the crack tip motion gives rather accurate results when compared to analytical solutions. In addition it proved to be a reasonable tool to investigate more general problems. In the

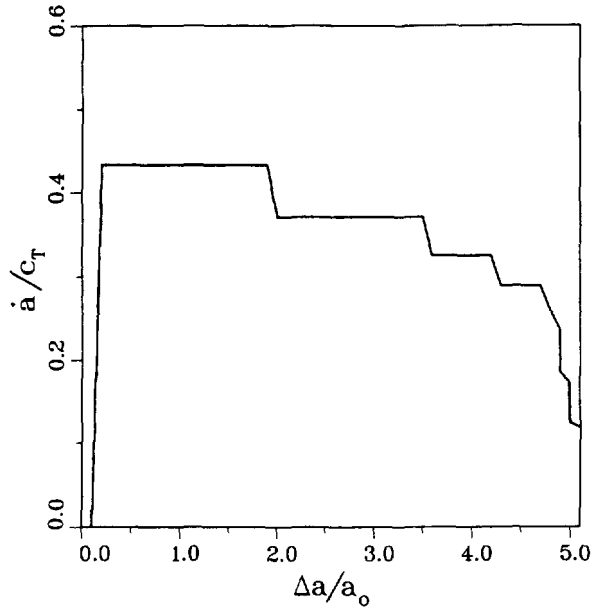

Fig. 11. Crack tip speed.

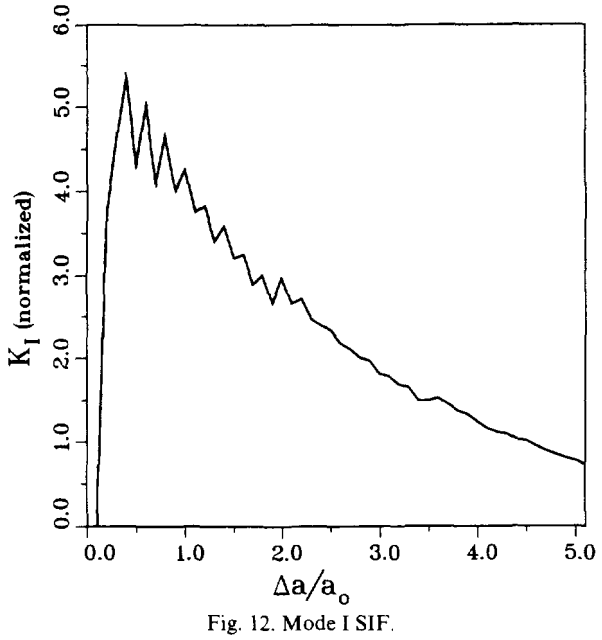

Fig. 12. Mode I SIF.

to crack arrest, can clearly be seen. The strong decrease in crack tip speed results not only from an increasing distance to the center of compression, but also from a change in geometry due to crack growth. The simulation here was stopped at $t = 27a_0/c_L$.

6. CONCLUSIONS

A numerical method has been presented, which enables the simulation of dynamic crack propagation under arbitrary loading conditions and along arbitrary crack paths. Since penetration of the crack faces is kinematically inadmissible, the treatment of the contact problem arising from crack closure is included in the procedure. Crack advance starting from a given initial crack is determined from a fracture criterion motivated by experimental observations. The method although being based on a rough approximation of the crack tip motion gives rather accurate results when compared to analytical solutions. In addition it proved to be a reasonable tool to investigate more general problems. In the

$$R_{\mathrm{L,T}} = \sqrt{c_{\mathrm{L,T}}^2 (t-\tau)^2 - r^2}$$

$$A_{\nu\gamma\varepsilon} = 2(\delta_{\nu\gamma} r_{,\varepsilon} + \delta_{\gamma\varepsilon} r_{,\nu} + \delta_{\nu\varepsilon} r_{,\gamma} - 4 r_{,\nu} r_{,\gamma} r_{,\varepsilon})$$

$$B^{\mathrm{L}}_{\nu\gamma\varepsilon} = (k^2 - 2)\delta_{\nu\gamma} r_{,\varepsilon} + 2 r_{,\nu} r_{,\gamma} r_{,\varepsilon}$$

$$B^{\mathrm{T}}_{\nu\gamma\varepsilon} = 2 r_{,\nu} r_{,\gamma} r_{,\varepsilon} - \delta_{\nu\varepsilon} r_{,\gamma} - \delta_{\gamma\varepsilon} r_{,\nu}$$

APPENDIX B: AUXILIARY FUNCTIONS

$$\int_{(n-1)\Delta t}^{(n+1)\Delta t} \rho u^G_{\nu\varepsilon}(\mathbf{y}; \mathbf{x}^d, t_m - \tau) \ddot{\eta}_n(\tau)\, \mathrm{d}\tau = \frac{1}{2\pi c_{\mathrm{T}} \Delta t} \sum_{i=-1}^{1} (-2)^{(1-i^2)} V_{\nu\varepsilon}(\mathbf{y}; \mathbf{x}^d, m, n, i)$$

$$\int_{(n-1)\Delta t}^{(n+1)\Delta t} \sigma^G_{\nu\gamma\varepsilon}(\mathbf{y}; \mathbf{x}^d, t_m - \tau) \eta_n(\tau)\, \mathrm{d}\tau = \frac{1}{2\pi c_{\mathrm{T}} \Delta t} \sum_{i=-1}^{1} (-2)^{(1-i^2)} \frac{1}{r} \Sigma_{\nu\gamma\varepsilon}(\mathbf{y}; \mathbf{x}^d, m, n, i)$$

$$\int_{(n-1)\Delta t}^{(n+1)\Delta t} \rho u^G_{33}(\mathbf{y}; \mathbf{x}^d, t_m - \tau) \ddot{\eta}_n(\tau)\, \mathrm{d}\tau = \frac{1}{2\pi c_{\mathrm{T}} \Delta t} \sum_{i=-1}^{1} (-2)^{(1-i^2)} \frac{\tilde{H}_{\mathrm{T}}}{\tilde{R}_{\mathrm{T}}}$$

$$\int_{(n-1)\Delta t}^{(n+1)\Delta t} \sigma^G_{3\gamma 3}(\mathbf{y}; \mathbf{x}^d, t_m - \tau) \eta_n(\tau)\, \mathrm{d}\tau = \frac{-1}{2\pi c_{\mathrm{T}} \Delta t} \sum_{i=-1}^{1} (-2)^{(1-i^2)} \frac{1}{r} r_{,\gamma} \tilde{H}_{\mathrm{T}} \tilde{R}_{\mathrm{T}}$$

where

$$V_{\nu\varepsilon}(\ldots) = (2 r_{,\nu} r_{,\varepsilon} - \delta_{\nu\varepsilon}) \frac{1}{r^2} \left[\frac{1}{k} \tilde{H}_{\mathrm{L}} \tilde{R}_{\mathrm{L}} - \tilde{H}_{\mathrm{T}} \tilde{R}_{\mathrm{T}} \right] + r_{,\nu} r_{,\varepsilon} \left[\frac{1}{k} \frac{\tilde{H}_{\mathrm{L}}}{\tilde{R}_{\mathrm{L}}} - \frac{\tilde{H}_{\mathrm{T}}}{\tilde{R}_{\mathrm{T}}} \right] + \delta_{\nu\varepsilon} \frac{\tilde{H}_{\mathrm{T}}}{\tilde{R}_{\mathrm{T}}}$$

$$\Sigma_{\nu\gamma\varepsilon}(\ldots) = \frac{1}{3} A_{\nu\gamma\varepsilon} \frac{1}{r^2} \left[\frac{1}{k^3} \tilde{H}_{\mathrm{L}} \tilde{R}_{\mathrm{L}}^3 - \tilde{H}_{\mathrm{T}} \tilde{R}_{\mathrm{T}}^3 \right] - B^{\mathrm{L}}_{\nu\gamma\varepsilon} \frac{1}{k^3} \tilde{H}_{\mathrm{L}} \tilde{R}_{\mathrm{L}} + B^{\mathrm{T}}_{\nu\gamma\varepsilon} \tilde{H}_{\mathrm{T}} \tilde{R}_{\mathrm{T}}$$

$$\tilde{H}_{\mathrm{L,T}} = H(c_{\mathrm{L,T}} \Delta t (m-n-i) - r)$$

$$\tilde{R}_{\mathrm{L,T}} = \sqrt{(c_{\mathrm{L,T}} \Delta t (m-n-i))^2 - r^2)}$$

$$\lim_{r \to 0} \frac{1}{r^2} \left(\frac{1}{k} \tilde{R}_{\mathrm{L}} - \tilde{R}_{\mathrm{T}} \right) = \frac{1}{2 c_{\mathrm{T}} \Delta t (m-n-i)} \left(1 - \frac{1}{k^2} \right)$$

$$\lim_{r \to 0} \frac{1}{r^2} \left(\frac{1}{k^3} \tilde{R}_{\mathrm{L}}^3 - \tilde{R}_{\mathrm{T}}^3 \right) = \frac{3}{2 c_{\mathrm{T}} \Delta t (m-n-i)} \left(1 - \frac{1}{k^2} \right)$$

$\Rightarrow$ Functions $V_{\nu\varepsilon}(\ldots)$ and $\Sigma_{\nu\gamma\varepsilon}(\ldots)$ are regular for $r \to 0$!